Mathematical Biosciences and Engineering

Research article

A GraphSAGE-based model with fingerprints only to predict drug-drug interactions

Bo Zhou[1,2,*], Bing Ran[3] and Lei Chen[3]

[1] Institute of Wound Prevention and Treatment, Shanghai University of Medicine and Health Sciences, Shanghai 201318, China

[2] School of Basic Medical Sciences, Shanghai University of Medicine and Health Sciences, Shanghai 201318, China

[3] College of Information Engineering, Shanghai Maritime University, Shanghai 201306, China

* **Correspondence:** Email: zhoub@sumhs.edu.cn; Tel: +8602165882815; Fax: +8602165882570.

Abstract: Drugs are an effective way to treat various diseases. Some diseases are so complicated that the effect of a single drug for such diseases is limited, which has led to the emergence of combination drug therapy. The use multiple drugs to treat these diseases can improve the drug efficacy, but it can also bring adverse effects. Thus, it is essential to determine drug-drug interactions (DDIs). Recently, deep learning algorithms have become popular to design DDI prediction models. However, most deep learning-based models need several types of drug properties, inducing the application problems for drugs without these properties. In this study, a new deep learning-based model was designed to predict DDIs. For wide applications, drugs were first represented by commonly used properties, referred to as fingerprint features. Then, these features were perfectly fused with the drug interaction network by a type of graph convolutional network method, GraphSAGE, yielding high-level drug features. The inner product was adopted to score the strength of drug pairs. The model was evaluated by 10-fold cross-validation, resulting in an AUROC of 0.9704 and AUPR of 0.9727. Such performance was better than the previous model which directly used drug fingerprint features and was competitive compared with some other previous models that used more drug properties. Furthermore, the ablation tests indicated the importance of the main parts of the model, and we analyzed the strengths and limitations of a model for drugs with different degrees in the network. This model identified some novel DDIs that may bring expected benefits, such as the combination of PEA and cannabinol that may produce better effects. DDIs that may cause unexpected side effects have also been discovered, such as the combined use of WIN 55,212-2 and cannabinol. These DDIs can provide novel insights for treating complex diseases or

avoiding adverse drug events.

1. Introduction

Disease is a great threat to human life. Researchers have attempted to design effective schemes for treating different diseases when they are discovered. For a long time, drugs have been deemed to be one of the most effective ways to treat various diseases. However, the utility of a single drug for treating complex diseases is limited as these diseases always involve multiple targets and one drug cannot target them at one time. In this case, combination drug therapy is a popular way to tackle this problem. Multiple drugs are taken at the same time, which can improve drug efficacy and reduce drug resistance [1]. However, this scheme also brings other problems. Some drugs can interact with others and this interaction can induce adverse drug events [2]. On one hand, such events are harmful to patients' health. On the other hand, they can lead to the withdrawal of drugs from the market, bringing great risks to pharmaceutical companies. Clearly, determination of drug-drug interactions (DDIs) is an important topic in drug research.

In vitro experiments and clinical trials are traditional ways to determine DDIs. However, these methods are of low efficiency and cannot give large-scale tests. Furthermore, the execution of these methods is expensive. In recent years, computational methods have become alternative ways to identify DDIs as these methods have some evident advantages, such as high efficiency and low cost. Among current computational methods for predicting DDIs, machine learning-based methods are an important portion. In early examples, investigators employed traditional machine learning algorithms to construct the prediction methods. For example, Chen et al. proposed a scheme to assess the similarity of two drugs and used the nearest neighbor algorithm to identify DDIs based on this scheme [3]. Cheng et al. employed support vector machines to identify DDIs, where each drug pair was represented by features derived from simplified molecular input line entry system (SMILES) formats of two drugs in the pair and their side effects [4]. Ran et al. adopted drug fingerprints and random forest to build a model for identifying DDIs [5]. Cheng et al. integrated the Gaussian interaction profile kernel on DDI profiles and the regularized least squares classifier to predict new DDIs [6]. Rohani and Eslahchi integrated multiple drug similarities to achieve high-level features which were fed into one neural network to train the DDI prediction model [7]. Recently, deep learning algorithms have been deemed to be more powerful than traditional machine learning algorithms and have been successfully applied to various fields [8–11]. For the prediction of DDIs, several deep learning-based methods have been proposed to date. He et al. proposed a multi-type feature fusion based on graph neural networks for the prediction of DDIs [12]. Yan et al. extracted unified drug mapping features from five drug-related heterogeneous information sources and employed deep neural networks to infer DDIs [13]. Lin et al. proposed a model to predict DDI events using multi-source drug fusion, multi-source feature fusion, and the transformer self-attention mechanism [14]. Feng et al. extracted drug features from a DDI network via a graph convolution network and adopted the deep neural network to make predictions [15]. Liu et al. learnt drug representations from multiple drug feature networks, accessed drug pair features through an attention neural network, and finally used a deep neural network to make predictions [16]. Most

current deep learning-based methods require various drug information. Although their performance is excellent, their application is a problem as some types of drug information may not be available for some drugs. Thus, it is necessary to design a deep learning-based method for predicting DDIs which only needs commonly used drug information. This information should be analyzed by a certain deep learning algorithm so that an efficient model can be built.

In this study, a new deep learning-based model was built to predict DDIs. Different from previous deep learning-based models, this model only adopts drug fingerprints, which enhances its application values. With validated DDIs sourced from DrugBank [17,18], a drug network was built, which was fed into the GraphSAGE [19] along with the drug features derived from their fingerprints. Based on the high-level drug features yielded by GraphSAGE, the score of two drugs was calculated via inner product, measuring the likelihood of the interaction between them. The 10-fold cross-validation results indicated that the model had high performance, which was better than the previous model directly using drug fingerprint features. This performance was also competitive compared with some previous powerful models. Furthermore, we elaborated the reasonability of the model architecture, and analyzed the strengths and limitations of the model. Finally, some latent DDIs inferred by this model were analyzed to prove its prediction ability.

2. Materials and methods

2.1. Dataset

The DDI dataset used in this study was retrieved from Ran et al.'s study [5]. This dataset contains 37,496 DDIs, involving 722 experimental validated drugs. These DDIs were extracted from the DDIs reported in DrugBank (https://go.drugbank.com/) [17,18], a well-known dataset containing information on drugs and drug targets. They were regarded as positive samples in this study. The 37,496 DDIs can be indicated by a matrix with 722 rows and 722 columns, denoted as A. $A_{ij} = 1$ if and only if the i-th drug d_i and j-th drug d_j can interact with each other.

To obtain pattern that can identify positive samples, the negative samples were necessary. However, no public datasets collected the validated pairs of drugs that have been determined not to be actual DDIs because they lacked practical applications. The unlabeled pairs of drugs can be latent negative samples. However, they were 222,785 unlabeled pairs, which were much greater in number than the positive samples. In this study, we randomly selected as many unlabeled pairs as there were positive samples, and labeled these the negative samples. The above positive and negative samples constituted a dataset, denoted as S.

2.2. Drug network

In recent years, networks have been deemed a powerful method to investigate various biological problems [20–24] because they can systematically organize all objects and overview each object with all other objects in the background. Here, we also adopted such a method to investigate DDIs.

As the investigated DDIs covered 722 drugs, they were defined as nodes in the constructed network. As for the edges in this network, they were determined by the 37,496 positive samples. In detail, for two nodes in the network, if their corresponding drugs can comprise a positive sample, they were connected by an edge. Therefore, the constructed network contained 722 nodes and 37,496 edges.

To show the topological structure of this network, we counted the degree of each node, indicating the number of DDIs containing each drug, as shown in Figure 1. It can be found that some nodes have high degrees, suggesting that the corresponding drugs can interact with many other drugs. Most nodes have degrees lower than 200. The media number was 82 and the average number was 103.87. For convenience, this network was denoted as *N*. The proposed model can infer new connections (latent DDIs) based on the currently known DDIs.
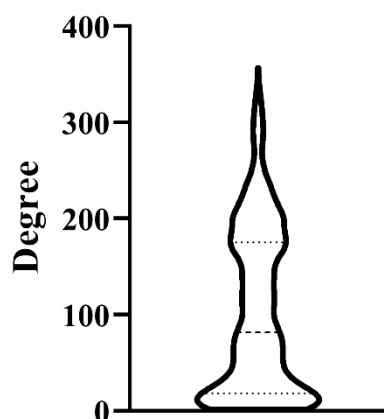
Figure 1. A violin plot to show the distribution of degrees of nodes in the constructed network. Some nodes have high degrees, indicating that they can interact with many other drugs.

2.3. Drug fingerprint

Fingerprint is widely used in investigation on drug-related problems. Different from the fingerprint of human, which is always modeled as an image processing problem [25,26], a fingerprint for drugs or chemicals is a substructure, which is originally designed to assist in chemical database substructure searching [27]. Later, it was found to be useful for chemical clustering and classification. Based on the fingerprints of a given drug, the drug can be represented by a numeric vector. Although this representation seems an ordinary form to represent drugs, models based on it always provide good performance. Here, we also adopted this form to build the original representation of drugs. In detail, the SMILES formats of 722 drugs were first sourced from DrugBank. Then, the RDKit (http://www.rdkit.org) was adopted to extract the ECFP_4 fingerprint [28] from these formats. This type of fingerprint involves several special substructures, which are generated by the following processes:

First, the Daylight atomic invariants rule is used to assign an integer identifier to each atom in a molecule. This rule considers six properties of an atom, including the number of immediate non-hydrogen neighbors, the valence minus the number of hydrogens, the atomic number, the atomic mass, the atomic charge, and the number of attached hydrogens (both implicit and explicit). In ECFP features, a seventh attribute is commonly used to indicate whether an atom is contained in at least one ring. The given features are then converted into integer values using a hash function, which acts as the initial identifiers of the atoms.

Then, the identifier is updated iteratively to include information about the atom's neighborhood,

including the type of bond (single, double, triple, or aromatic) that connects the atom. Each atom collects its own identifier and the identifiers of neighboring atoms into an array. A hash function is then applied to reduce this array to a new single integer identifier. After generating new identifiers for all atoms, they replace the old ones and are added to the fingerprint set. This process is repeated a predefined number of times.

Once completed, any duplicate identifiers in the fingerprint set are removed, leaving only the remaining integer identifiers to define the ECFP.

Finally, a binary vector is constructed for each drug based on its ECFP_4 fingerprints. Each component in this vector indicates the presence and absence of a certain substructure. It is set to 1 if the drug has the corresponding substructure; otherwise, it is set to 0. Here, the ECFP_4 fingerprint contains 1024 substructures. Thus, each drug d is represented by a 1024-dimensional binary vector, formulated by

$$v_d = [f_1, f_2, \cdots, f_{1024}]^T. \tag{1}$$

Clearly, this vector contains which substructures the drug d has, reflecting its entire structure. The feature vectors of 722 drugs are aggregated in a matrix, denoted by FM_F, where the i-th row is the feature vector of the i-th drug.

2.4. GraphSAGE

In Sections 2.2 and 2.3, two types of drug properties were introduced. For drug fingerprint, it can be deemed as providing linear information of drugs, whereas the drug network provides non-linear information of drugs. Proper fusion of these two types of drug properties was helpful to access high-level drug features. Recently, node embedding learning has been a hot topic in machine learning. The main purpose of this method is to assign an informative feature vector to each node in a given network. Graph convolutional networks (GCNs) [29] are one of the powerful algorithms in this field and has wide applications in bioinformatics [30–33]. Here, one of its variants, named GraphSAGE [19], was employed. This algorithm was applied to the drug network N and the feature vectors of drugs mentioned in Section 2.3 was set as its input. Based on N and the original feature vectors of the drugs, we attempted to access more informative feature vectors of drugs.

The main idea of GraphSAGE is to efficiently aggregate feature information from a node's local neighborhood, thereby generating a more informative feature representation of the node. Different from GCN, which always considers all direct neighbors, GraphSAGE samples a fixed-size set of neighbors, called local neighborhood. This operation can decrease the computational complex of the algorithm. For node v, its local neighborhood is denoted as $N(v)$. Generally, the aggregation procedures can be run for K rounds, which determines the search depth. In the k-th round, an aggregation function is employed, denoted by $AGGREGATE_k$. The feature vectors of the neighbors in the local neighborhood of v are aggregated using this aggregation function, formulated as

$$h_{N(v)}^k = AGGREGATE_k(\{h_u^{k-1} : u \epsilon N(v)\}), \tag{2}$$

where h_u^{k-1} is the feature vector of u after the (k-1)-th round. Specifically, h_u^0 is the input feature vector of u. This aggregated feature vector is concatenated to the feature vector of v after the (k-1)-th round, which is further refined by a fully connected layer with a nonlinear activation function σ,
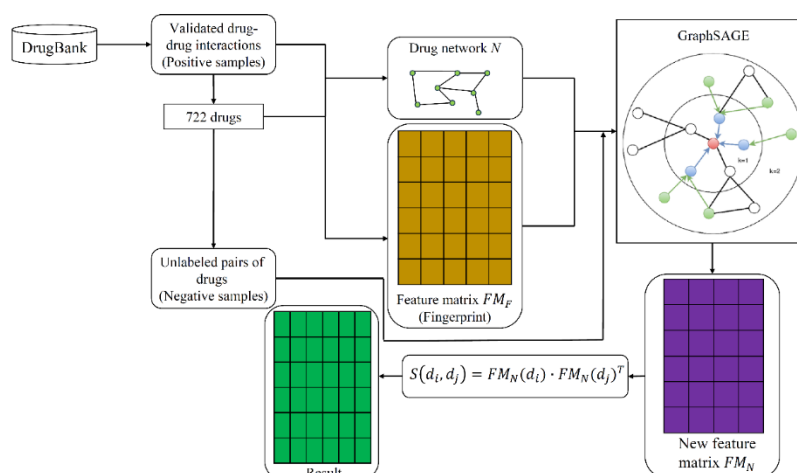
formulated as

$$h_v^k = \sigma(W^k \cdot CONCAT(h_v^{k-1}, h_{N(v)}^k)),\tag{3}$$

where W^k $(k \in \{1,2,\cdots,K\})$ is a weight matrix, which can be trained. At the end of the k-th round, h_v^k is updated to $h_v^k/\|h_v^k\|_2$.

2.5. Model architecture

In this study, a model based on GraphSAGE was proposed to identify DDIs. The entire procedure is illustrated in Figure 2.

Figure 2. Entire procedures of the GraphSAGE-based model to predict drug-drug interactions. The validated drug-drug interactions are retrieved from DrugBank, termed as positive samples. The negative samples are randomly selected from unlabeled drug pairs. To access informative drug features, the original fingerprint features and the drug interaction network are fed into GraphSAGE. The inner product is applied to the refined drug features to assess the linkage of two drugs.

First, the validated DDIs retrieved from DrugBank were used to construct the drug network N as described in Section 2.2. At the same time, the ECFP_4 fingerprints of 722 drugs were extracted, which were used to generate the feature matrix FM_F. Then, the above network and feature matrix were fed into GraphSAGE to produce the new feature matrix FM_N of 722 drugs. In this procedure, the selected unlabeled pairs of drugs (i.e., negative samples) were employed to train the parameters in GraphSAGE, thereby accessing more powerful drug features. The i-th row of FM_N was the new feature vector of the drug d_i. Based on the new feature representations of drugs, the score between drugs d_i and d_j was calculated by the inner product of their feature vectors, formulated as

$$S(d_i, d_j) = FM_N(d_i) \cdot FM_N(d_j)^T.\tag{4}$$

If this score is larger than a predefined threshold, d_i and d_j were predicted to interact with each

other, i.e., they comprised a DDI (positive sample); otherwise, they were predicted to constitute a negative sample.

Loss function and optimization. There are some parameters that can be trained in GraphSAGE (e.g., the weight matrices in the aggregation procedure). These were optimized by standard stochastic gradient descent and backpropagation techniques. As a binary classification problem, we selected the binary cross entropy as the loss function, which is defined as

$$L = -\sum(y \log p(x) + (1-y)\log(1-p(x))), \tag{5}$$

where $p(x)$ is the prediction of x yielded by the model and y is the true label. The optimization procedure was implemented using the Adam optimizer [34].

The proposed model mainly used the GraphSAGE to access high-level drug features. Its time complexity was the same as GraphSAGE. According to the original reference of GraphSAGE [19], its time complexity is $O(\prod_{i=1}^{K} S_i)$, where K is the number of rounds in aggregation procedures and S_i is the fixed number of sampling neighbors in the i-th round.

2.6. Performance evaluation

Cross-validation methods have wide applications in evaluating the performance of classification models [35]. In this method, samples are equally and randomly divided into several parts. Each part is picked up to comprise the test dataset one by one, whereas the rest of the parts constitute the training dataset. The model based on the training dataset is applied to the test dataset to assess its performance. Generally, most studies opt to divide samples into five or ten parts, i.e., 5 or 10-fold cross-validation. Here, we selected 10-fold cross-validation to test the performance of constructed models. In each round of the cross-validation, some edges, corresponding to the positive samples in the test dataset, in the drug network N were discarded. This can strictly isolate the information of test samples from training the model.

To determine the prediction quality of cross-validation results, several measurements have been proposed for binary classification problems. This study adopted the following measurements: precision, recall, overall accuracy (ACC), F1-measure [22,36–42], and Matthews correlation coefficient (MCC) [43], which can be computed by

$$Precision = \frac{TP}{TP+FP}, \tag{6}$$

$$Recall = \frac{TP}{TP+FN}, \tag{7}$$

$$F1 - measure = \frac{2 \times Recall \times Precision}{Recall + Precision}, \tag{8}$$

$$ACC = \frac{TP+TN}{TP+FP+TN+FN}, \tag{9}$$

$$MCC = \frac{TP \times TN - FP \times FN}{\sqrt{(TP+FP) \times (TP+FN) \times (TN+FP) \times (TN+FN)}}, \tag{10}$$

where TP/TN stands for true positives/negatives, and FP/FN represents false positives/negatives.

In addition, we employed the receiver operating characteristic (ROC) and precision-recall (PR) curves to fully display the performance of classification models under different thresholds. The ROC curve defines the true positive rate (same as recall) as the Y-axis and the false positive rate (i.e., $\frac{FP}{TN+FP}$) as the X-axis. The PR curve is drawn by defining recall as the X-axis and precision as the Y-axis. The area under the above two curves, denoted by AUROC and AUPR, are important measurements to assess the quality of predicted results. They were given along with the curves in this study.

3. Results and discussion

In this study, we designed a new model for predicting DDIs. The entire procedure is illustrated in Figure 1. This section reports the performance of the model and elaborates on its reasonability, superiority, and limitations. Furthermore, the latent DDIs identified by the model are analyzed.
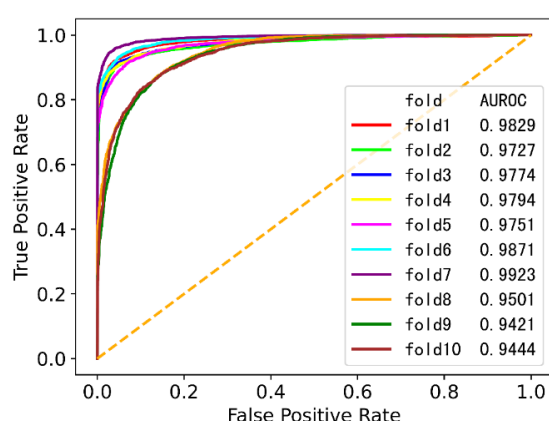
3.1. Parameter setting

In the GraphSAGE-based model, some parameters should be determined. All parameters were related to GraphSAGE. First, the aggregation procedures in GraphSAGE were executed in two rounds, i.e., $K = 2$. In this case, the features of 2-neighbors can be aggregated to the target node. Second, the mean aggregator was selected to aggregate neighbors' features, i.e., Eqs (2) and (3) were combined and detailed as

$$h_v^k = \sigma\left(W^k \cdot MEAN(\{h_v^{k-1}\} \cup \{h_u^{k-1} : u \epsilon N(v)\})\right). \tag{11}$$

Finally, the dimensions of output features in two aggregation procedures were set to 128 and 16, i.e., the sizes of W^1 and W^2 were 128×1024 and 16×128, respectively.

3.2. Performance of the GraphSAGE-based model

fold	AUROC
fold1	0.9829
fold2	0.9727
fold3	0.9774
fold4	0.9794
fold5	0.9751
fold6	0.9871
fold7	0.9923
fold8	0.9501
fold9	0.9421
fold10	0.9444

Figure 3. ROC curves of the GraphSAGE-based model under 10-fold cross-validation. The AUROC values vary between 0.9400 and 0.9950, suggesting the high performance of the model.
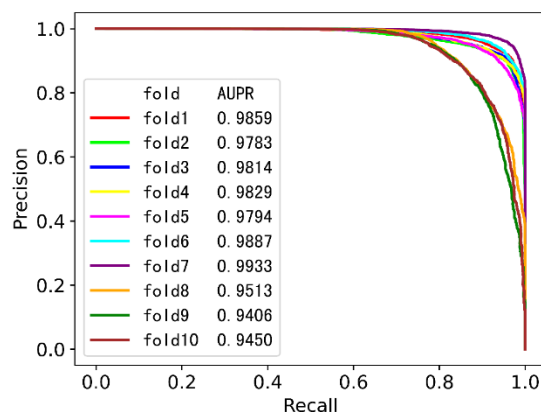
Figure 4. PR curves of the GraphSAGE-based model under 10-fold cross-validation. The AUPR values vary between 0.9400 and 0.9950, implying the high performance of the model.

With the parameter setting mentioned in Section 3.1, the GraphSAGE-based model was evaluated by 10-fold cross-validation. The ROC and PR curves are illustrated in Figures 3 and 4, respectively. It can be found that each ROC or PR curve under one fold was nearly perfect. According to the AUROC and AUPR values in these two figures, AUROC values on ten folds changed between 0.9400 and 0.9950, and the AUPR values varied in the same interval. These results suggested the high performance of the model.

In the GraphSAGE-based model, we used the inner product to finally measure the linkage of two drugs. A threshold of 0 can be deemed as a natural choice to determine DDIs, i.e., drug pairs with scores higher than zero were predicted as positive samples; otherwise, they were identified as negative samples. Thus, we counted the measurements under this threshold, which are listed in Table 1. The average precision and recall were 0.967 and 0.798, respectively. The precision was quite high, whereas recall was not very satisfactory. The low recall meant that several positive samples were predicted as negative samples. As for the overall measurements, ACC, F1-measure, and MCC, these were around 0.861, 0.874, and 0.739, respectively. Such performance is acceptable. Thus, it was suggested to use this threshold to determine DDIs.

Table 1. Performance of the GraphSAGE-based model under 10-fold cross-validation.

Fold index	Precision	Recall	ACC	F1-measure	MCC
1	0.980	0.826	0.887	0.897	0.788
2	0.969	0.776	0.845	0.862	0.712
3	0.977	0.761	0.835	0.856	0.699
4	0.976	0.789	0.857	0.872	0.735
5	0.975	0.787	0.856	0.871	0.733
6	0.985	0.819	0.884	0.895	0.784
7	0.991	0.834	0.897	0.905	0.808
8	0.933	0.811	0.857	0.867	0.723
9	0.942	0.794	0.849	0.861	0.709
10	0.944	0.783	0.841	0.856	0.697
Mean	0.967	0.798	0.861	0.874	0.739

3.3. Ablation tests

The proposed GraphSAGE-based model has several parts. This section conducts some ablation tests to show the contribution of each part.

GraphSAGE is the most important part of the model, and is in charge of generating high-level drug features. Here, we removed this part to reconstruct the model. In this model, the drug fingerprint features (cf. Eq (1)) were directly fed into the scoring scheme (cf. Eq (4)) to measure the interaction likelihood of two drugs. This model was also assessed using 10-fold cross-validation, generating an AUROC of 0.5621 and AUPR of 0.5469, as listed in Table 2. Evidently, such performance was much lower than the GraphSAGE-based model, proving the importance of GraphSAGE in improving the quality of drug features.

The proposed model adopted the inner product to assess the interaction likelihood of two drugs. To prove this selection was reasonable, we replaced it with the sum operation, i.e., Eq (4) was replaced with the following equation

$$S(d_i, d_j) = FM_N(d_i) + FM_N(d_j).$$ (12)

A model with this score scheme was built and also evaluated by 10-fold cross-validation, yielding the AUROC and AUPR, listed in Table 2. It can be found that the AUROC was 0.7174, whereas the AUPR was 0.6388. They were also much lower than those of the GraphSAGE-based model, which were all higher than 0.97. This result indicated that the inner product was more effective than the sum operation to capture the interaction strength of two drugs.

Table 2. Performance of the model by changing its main parts.

Object	Operation	AUROC	AUPR
GraphSAGE	Removal	0.5621	0.5469
Scoring scheme	Replacement	0.7174	0.6388

3.4. Analysis of the model

With the above arguments, the GraphSAGE-based model demonstrated high performance in identifying DDIs. However, its performance on different drugs may not be the same. As shown in Figure 1, the degrees of nodes in the drug network covers a large range, suggesting that some drugs can interact with many drugs, whereas others can interact with only a few drugs. It was interesting to investigate the performance of the GraphSAGE-based model on the above two drug groups. In view of this, the 722 drugs were equally divided into two groups according to their degrees in the network. The first group contained the drugs with high degrees, whereas the second group consisted of other drugs with low degrees. For convenience, they are called the high and low groups. Accordingly, three DDI groups were constructed, named high-high, high-low and low-low groups. Evidently, the high-high group contained DDIs with two drugs in the high group, the low-low group consisted of DDIs with two drugs in the low group, and the high-low group included DDIs with one drug in the high group and one drug in the low group. For the cross-validation results of the GraphSAGE-based model, its performance on the three DDI groups was individually counted, yielding the AUROC and AUPR values listed in Table 3. These two values for the high-high group were 0.9894 and 0.9967, respectively.

They decreased to 0.9461 and 0.8176 for the high-low group. As for the low-low group, they further dropped to 0.6020 and 0.2439. Clearly, the performance on the high-high group was highest, followed by that of the high-low and low-low groups. It was indicated that the GraphSAGE-based model had strong prediction ability on drugs that have been confirmed to interact with many other drugs, whereas its prediction ability on drugs that can interact with few drugs was relatively weak. This result was reasonable because drugs that can interact with many other drugs, which have high degrees in the drug network, can receive abundant information of its neighbors via GraphSAGE, which largely improved their representations, whereas the improvement for drugs that can interact with few drugs was limited.

Table 3. Performance of the model on three DDI groups.

Group	AUROC	AUPR
High-high group	0.9894	0.9967
High-low group	0.9461	0.8176
Low-low group	0.6020	0.2439

3.5. Comparison with the previous models

To show the superiority of the GraphSAGE-based model, we compared it with one previous model [5]. This model was built on the same dataset and also evaluated by 10-fold cross-validation. It directly adopted the drug fingerprint features to generate the representation of DDIs and selected the random forest as the prediction engine. The performance of this model and our model is listed in Table 4. It can be observed that our GraphSAGE-based model provided higher AUROC and AUPR than the previous model. The improvement was about 1%. As mentioned above, drug fingerprint features were directly adopted to constitute the features of DDIs. Such features were not very informative. The GraphSAGE-based model fused the drug fingerprint features and drug network information, containing more informative properties of drugs. This was the main reason why the GraphSAGE-based model was superior to this previous model.

Table 4. Comparison with the previous models.

Model	AUROC	AUPR
GraphSAGE-based model	0.9704	**0.9727**
Ran et al.'s model [5]	0.9629	0.9601
NDD [7]	0.9940	0.9470
DDIMDL [2]	**0.9979**	0.9208
DPDDI [15]	0.9560	0.9070
DANN-DDI [16]	0.9763	0.9709

As mentioned in Section 1, several DDI prediction models have been proposed. We selected four models (DDIMDL [2], NDD [7], DPDDI [15], and DANN-DDI [16]) for further comparing with our model, where DDIMDL, DPDDI, and DANN-DDI were constructed using deep learning algorithms. The performance of the above models is listed in Table 4. It can be observed that the proposed model provided the highest AUPR, whereas the AUROC of our model was lower than that of those three models. This result indicates that the proposed model provided competitive performance compared

with these previous models. Although the proposed model only adopted drug fingerprints, GraphSAGE perfectly fused the drug fingerprints and currently known DDI information, represented by the drug network. None of previous models can fuse these two types of information so perfectly. They employed more drug properties, such as target, pathway, etc., which enhanced their performance. However, this also induced the application problem because the properties of some drugs were not available. Anyway, the proposed model had special merits. The high performance guaranteed the reliability of its prediction and low number of required properties made the model more widely applicable.

3.6. Case study

Table 5. Top 20 predicted drug-drug interactions.

Index	Drug 1		Drug 2		Score
	DrugBank ID	Name	DrugBank ID	Name	
1	DB14043	Palmidrol	DB14737	CBN	180.046
2	DB13950	WIN 55212-2	DB14737	CBN	95.248
3	DB01482	Fenethylline	DB02377	Guanine	31.747
4	DB02377	Guanine	DB14132	8-chlorotheophylline	30.833
5	DB01384	Paramethasone	DB14681	Cortisone	29.575
6	DB02377	Guanine	DB13592	Etamiphylline	29.345
7	DB02377	Guanine	DB13203	Bamifylline	29.007
8	DB03322	Dexpropranolol	DB08807	Bopindolol	28.920
9	DB13856	Fluclorolone	DB14681	Cortisone	27.811
10	DB02377	Guanine	DB13449	Proxyphylline	27.800
11	DB02377	Guanine	DB13634	Pentifylline	27.696
12	DB03322	Dexpropranolol	DB13530	Mepindolol	27.084
13	DB01384	Paramethasone	DB14633	Prednisolone hemisuccinate	26.853
14	DB13843	Cloprednol	DB14681	Cortisone	26.431
15	DB03322	Dexpropranolol	DB06726	Bufuralol	25.731
16	DB02377	Guanine	DB13812	Bufylline	25.679
17	DB13856	Fluclorolone	DB14633	Prednisolone hemisuccinate	25.640
18	DB02377	Guanine	DB13573	Acefylline	24.828
19	DB01482	Fenethylline	DB01978	7,9-Dimethylguanine	24.747
20	DB02134	Xanthine	DB02377	Guanine	24.545

This section presents case studies to further demonstrate the generalization ability of

GraphSAGE-based model for predicting unknown DDIs in reliable databases and literature. Table 5 shows the 20 drug pairs with the highest predicted scores (Eq (4)).

3.6.1. Cannabinol (CBN)-related DDIs (palmidrol/CBN and WIN 55,212-2 (WIN)/CBN)

Among the predicted DDIs, palmidrol/CBN ranked first among all predicted DDIs with a significantly high score. CBN is the first cannabis compound purified from the ancient medicinal plant *Cannabis sativa*. Over 120 phytocannabinoids have been isolated from *Cannabis* plants, including one of the main and most recognized representatives, tetrahydrocannabinol (THC) [44]. Research has demonstrated that CBN binds to two members of the G protein-coupled receptor family, namely cannabinoid receptors 1 (CB1R) and 2. It is involved in various physiological conditions and human diseases associated with the endocannabinoid system (ECS) [45,46]. CBN is a non-enzymatic oxidation byproduct of THC. Although CBN has the same mechanism of action as THC, it has been poorly studied and is currently limited to phase II clinical trials in epidermolysis bullosa [47]. Therefore, predicting the drug interactions of CBN is useful for its clinical development and application.

Palmidrol (Palmitoylethanolamide, PEA) is an endogenous fatty acid amine that mimics several endocannabinoid-driven activities. It is primarily known for its anti-inflammatory, analgesic, and neuroprotective properties [48]. PEA cannot be considered a classic endocannabinoid as it does not bind the classical cannabinoid receptors CB1 and CB2. However, it may have a multi-modal mechanism of action primarily through the activation of the ligand-operated transcription factor PPAR-α. It also indirectly stimulates the effects of both phyto- or endocannabinoids through the ECS, thus targeting similar pathways as cannabinoids [49]. In addition, PEA may enhance the physiological activity of THC by increasing its affinity for a receptor and inhibiting its metabolic degradation. This phenomenon is referred to as the 'entourage effect', which suggests that PEA indirectly enhances the biological effects of endocannabinoids and phytocannabinoids [50,51]. Therefore, taking PEA and CBN together may provide greater benefits than taking them separately [52,53], which supports the predictions of our model.

WIN 55,212-2 (WIN)/CBN had the second-highest predictive score for the drug-drug interaction pair, after palmidrol/CBN. WIN is a synthetic aminoalkylindole derivative that is commonly used as a pharmacological tool to study the biological activity of cannabinoid receptors [54]. The mechanism of action of WIN may involve acting as a full agonist at the CB1 cannabinoid receptor with much higher affinity than THC for this receptor [55,56]. Additionally, it has been shown to activate other receptors including PPARα and PPARγ nuclear receptors [57]. Recent research has further confirmed the mechanism of anti-inflammatory activity of WIN independent of CB1, suggesting that alternative receptors mediate the effects of WIN [54,58]. To the best of our knowledge, there is currently no available data demonstrating the use of WIN in combination with other drugs, including CBN. However, scholars have also taken note of the potential negative side effects of cannabinoid-based drugs in treating several chronic diseases, such as epilepsy, chronic pain, multiple sclerosis, and neurodegenerative diseases [59–62]. Studies have shown that WIN, due to its aminoalkylindole-type structure, can significantly block G protein-coupled inward rectifier potassium channels 1 (GIRK1) and 2 (GIRK2) activated by CB1 or CB2 under high concentrations [63]. This helps to explain the adverse effects induced by WIN in vivo. However, this blocking effect was not observed in other typical cannabinoids similar in structure to CBN [63]. It is possible that the occurrence of adverse reactions may increase when WIN is used in combination with CBN.
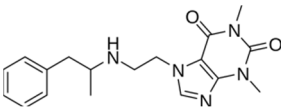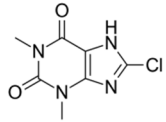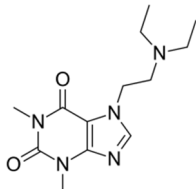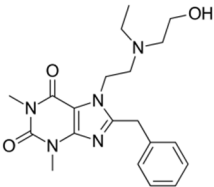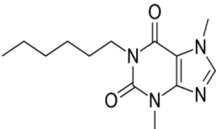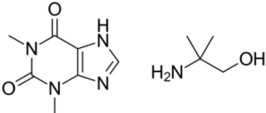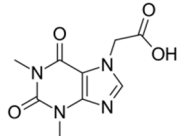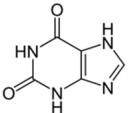
3.6.2. Guanine-related DDIs

Table 5 shows that Guanine may interact with nine drugs, including Fenethylline and Bufylline, as well as seven xanthine chemical drugs: 8-chlorotheophylline, Etamiphylline, Bamifylline, Proxyphylline, Pentifylline, Acefylline, and Xanthines. These drugs are competitive nonselective phosphodiesterase inhibitors and nonselective adenosine receptor antagonists, and are commonly used as mild stimulants and bronchodilators. As both Fenethylline [64] and Bufylline contain theophylline, a member of the xanthine family, and the nine drugs are discussed together.

According to DrugBank, the nine drugs are classified as experimental drugs, also known as discovery or pre-discovery stage drugs, which have not yet entered clinical trials or are not formally considered as candidate drugs. However, our prediction model suggests that they may interact with guanine, which could be explained by evidence from the drug structure. Guanine (G) is one of the four main nucleobases found in the nucleic acids DNA and RNA, along with adenine, cytosine, and thymine (uracil in RNA). In DNA, guanine pairs with cytosine. Guanine can be deaminated, releasing the amino group as ammonia, to form Xanthine. Xanthines form methylxanthines by adding methyl groups at different positions. This includes the nine drug classes mentioned earlier, as well as theophylline (also known as 1,3-dimethylxanthine) and theobromine (also known as 3, 7-dimethylxanthine). Table 6 shows synthetic methylxanthines used as drugs that have functional groups other than the methyl group. Johnson et al. conducted a study using ultraviolet absorption and Fourier transform infrared (FTIR) spectroscopic methods to investigate the interaction between naturally occurring methylxanthines (such as theophylline, theobromine, and caffeine) and DNA. The study revealed that theophylline, theobromine, and caffeine interact with all the base pairs of DNA (A-T; G-C) and phosphate groups through hydrogen bond (H-bond) interactions [65]. Our model's prediction is consistent with the observation that nine purine derivative drugs interact with guanine in a similar manner.

3.6.3. Corticosteroid-related DDI

We also noted the following drug pairs in Table 5, Paramethasone/Cortisone; Fluclorolone/Cortisone; Paramethasone/Prednisolone hemisuccinate; Cloprednol/Cortisone; Fluclorolone/Prednisolone hemisuccinate, etc. These drugs belong to a class of steroid hormones that can bind with the cortisol receptor and trigger various metabolic, immunes and homeostatic effects [66]. They are also molecules that inhibit leukocyte infiltration during inflammation, interfere with inflammation response, and suppress humoral immune responses [67]. Our prediction model assigned higher prediction scores for Corticosteroid-related DDI, which may be due to the increased risk or severity of adverse reactions when drugs of the same class are used in combination.

Table 6. Drug structures of guanine-related DDIs.

Guanine	Drugs predicted to interact with guanine	Score
	Fenethylline	31.747
	8-chlorotheophylline	30.833
	Etamiphylline	29.345
	Bamifylline	29.007
	Proxyphylline	27.800
	Pentifylline	27.696
	Bufylline	25.679
	Acefylline	24.828
	Xanthine	24.545
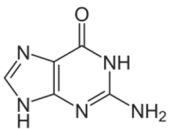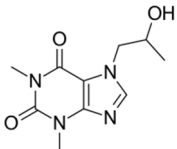
3.7. Clinical applications of the model

Clinical practice often requires the combined use of multiple drugs due to the complexity of diseases and the possibility that the human body may suffer from multiple diseases simultaneously. It is important to consider the potential risks and benefits of using multiple drugs and to monitor patients closely for any adverse effects. Although DDIs may have intended benefits, they can also result in unintended side effects or toxicities. For instance, studies on the combined use of PEA and CBN are

currently limited to animal experiments and phase II clinical trials for a single indication. However, it is predicted that this drug combination may yield better results. Another example is the combination of WIN and CBN, which has not yet been reported. It is also predicted that this combination may have corresponding side effects. This is supported by experimental evidence that WIN has varying effects on CB1 receptors at high concentrations.

In clinical practice, doctors can use this model for pre-combination questioning when considering new drug combinations, in addition to traditional drug combinations, to improve collaborative treatment effectiveness. This model can provide an analytical basis for the treatment of specific and complex diseases, as well as for different drug combinations targeting different diseases. If a potential high risk of DDI is predicted, doctors should remain vigilant and consult the latest research progress, such as animal experiments or clinical trials, to verify the situation. This is necessary to ensure patient safety and treatment effectiveness.

Effective methods for obtaining drug information are crucial for ensuring rational drug combinations in modern medicine. Clinicians and pharmacologists need to stay up-to-date with the latest developments in drug development to address the issue of rational drug combinations due to the constantly updated DDI data. This study can provide guidance for the development and implementation of clinical combination drug therapy.

3.8. Limitations of this study

Although the proposed model had high performance and wide applications, it also has some limitations. As mentioned above, the model had poor performance on drugs that can interact with few drugs. This was induced by the structure of the drug network, which was constructed by currently known DDIs. If other associations between drugs were combined, a more complete drug network can be built, thereby improving the quality of features of some drugs and further enhancing the performance of the model. As for the scalability of our model, this was also a problem. The model can only predict novel DDIs between drugs that can interact with at least one drug. If one novel drug has not been detected to interact with any other drugs, it cannot be included in the drug network. In this case, its high-level features cannot be accessed, influencing the predictions of DDIs involving this drug. In future, we will continue this work to set up more perfect models.

4. Conclusions

This study proposed a GraphSAGE-based model for predicting DDIs. By employing the GraphSAGE, drug fingerprint features and the drug interaction network were perfectly fused, thereby generating high-level drug features. The test results indicated that the model with these features provided high performance. It was superior to the model directly using drug fingerprint features and was competitive compared with other previous models. The model overcame the application problems because it used commonly used drug fingerprint features. Furthermore, the practical value of the GraphSAGE-based model was demonstrated by the case studies, which analyzed the latent DDIs discovered by the model. It is hopeful that the model can be a useful tool to identify novel DDIs.

Use of AI tools declaration

The authors declare they have not used artificial intelligence (AI) tools in the creation of this article.

Conflict of interest

The authors declare there is no conflict of interest.

References

1. G. Lee, C. Park, J. Ahn, Novel deep learning model for more accurate prediction of drug-drug interaction effects, *BMC Bioinf.*, **20** (2019), 415. https://doi.org/10.1186/s12859-019-3013-0

2. Y. Deng, X. Xu, Y. Qiu, J. Xia, W. Zhang, S. Liu, A multimodal deep learning framework for predicting drug-drug interaction events, *Bioinformatics*, **36** (2020), 4316–4322. https://doi.org/10.1093/bioinformatics/btaa501

3. L. Chen, C. Chu, Y. H. Zhang, M. Zheng, L. Zhu, X. Kong, et al., Identification of drug-drug interactions using chemical interactions, *Curr. Bioinf.*, **12** (2017), 526–534. https://doi.org/10.2174/1574893611666160618094219

4. F. Cheng, Z. Zhao, Machine learning-based prediction of drug–drug interactions by integrating drug phenotypic, therapeutic, chemical, and genomic properties, *J. Am. Med. Inf. Assoc.*, **21** (2014), e278–e286. https://doi.org/10.1136/amiajnl-2013-002512

5. B. Ran, L. Chen, M. Li, Y. Han, Q. Dai, Drug-drug interactions prediction using fingerprint only, *Comput. Math. Methods Med.*, **2022** (2022), 7818480. https://doi.org/10.1155/2022/7818480

6. C. Yan, G. Duan, Y. Pan, F. X. Wu, J. Wang, DDIGIP: Predicting drug-drug interactions based on Gaussian interaction profile kernels, *BMC Bioinf.*, **20** (2019), 538. https://doi.org/10.1186/s12859-019-3093-x

7. N. Rohani, C. Eslahchi, Drug-drug interaction predicting by neural network using integrated similarity, *Sci. Rep.*, **9** (2019), 13645. https://doi.org/10.1038/s41598-019-50121-3

8. A. M. Roy, J. Bhaduri, DenseSPH-YOLOv5: An automated damage detection model based on DenseNet and Swin-Transformer prediction head-enabled YOLOv5 with attention mechanism, *Adv. Eng. Inf.*, **56** (2023), 102007. https://doi.org/10.1016/j.aei.2023.102007

9. S. Jamil, A. M. Roy, An efficient and robust Phonocardiography (PCG)-based Valvular Heart Diseases (VHD) detection framework using Vision Transformer (ViT), *Comput. Biol. Med.*, **158** (2023), 106734. https://doi.org/10.1016/j.compbiomed.2023.106734

10. A. M. Roy, J. Bhaduri, T. Kumar, K. Raj, WilDect-YOLO: An efficient and robust computer vision-based accurate object localization model for automated endangered wildlife detection, *Ecol. Inf.*, **75** (2023), 101919. https://doi.org/10.1016/j.ecoinf.2022.101919

11. B. Jiang, S. Chen, B. Wang, B. Luo, MGLNN: Semi-supervised learning via multiple graph cooperative learning neural networks, *Neural Networks*, **153** (2022), 204–214. https://doi.org/10.1016/j.neunet.2022.05.024

12. C. He, Y. Liu, H. Li, H. Zhang, Y. Mao, X. Qin, et al., Multi-type feature fusion based on graph neural network for drug-drug interaction prediction, *BMC Bioinf.*, **23** (2022), 224. https://doi.org/10.1186/s12859-022-04763-2

13. X. Y. Yan, P. W. Yin, X. M. Wu, J. X. Han, Prediction of the drug-drug interaction types with the unified embedding features from drug similarity networks, *Front. Pharmacol.*, **12** (2021), 794205. https://doi.org/10.3389/fphar.2021.794205

14. S. Lin, Y. Wang, L. Zhang, Y. Chu, Y. Liu, Y. Fang, et al., MDF-SA-DDI: Predicting drug-drug interaction events based on multi-source drug fusion, multi-source feature fusion and transformer self-attention mechanism, *Briefings Bioinf.*, **23** (2022), bbab421. https://doi.org/10.1093/bib/bbab421

15. Y. H. Feng, S. W. Zhang, J. Y. Shi, DPDDI: A deep predictor for drug-drug interactions, *BMC Bioinf.*, **21** (2020), 419. https://doi.org/10.1186/s12859-020-03724-x

16. S. Liu, Y. Zhang, Y. Cui, Y. Qiu, Y. Deng, Z. Zhang, et al., Enhancing drug-drug interaction prediction using deep attention neural networks, *IEEE/ACM Trans. Comput. Biol. Bioinf.*, **20** (2023), 976–985. https://doi.org/10.1109/TCBB.2022.3172421

17. D. S. Wishart, C. Knox, A. C. Guo, D. Cheng, S. Shrivastava, D. Tzur, et al., DrugBank: A knowledgebase for drugs, drug actions and drug targets, *Nucleic Acids Res.*, **36** (2008), D901–D906. https://doi.org/10.1093/nar/gkm958

18. D. S. Wishart, C. Knox, A. C. Guo, S. Shrivastava, M. Hassanali, P. Stothard, et al., DrugBank: A comprehensive resource for in silico drug discovery and exploration, *Nucleic Acids Res.*, **34** (2006), D668–D672. https://doi.org/10.1093/nar/gkj067

19. W. Hamilton, Z. Ying, J. Leskovec, Inductive representation learning on large graphs, in *NIPS'17: Proceedings of the 31st International Conference on Neural Information Processing Systems*, (2017), 1024–1034.

20. X. Pan, L. Chen, I. Liu, Z. Niu, T. Huang, Y. D. Cai, Identifying protein subcellular locations with embeddings-based node2loc, *IEEE/ACM Trans. Comput. Biol. Bioinf.*, **19** (2022), 666–675. https://doi.org/10.1109/TCBB.2021.3080386

21. J. P. Zhou, L. Chen, Z. H. Guo, iATC-NRAKEL: An efficient multi-label classifier for recognizing anatomical therapeutic chemical classes of drugs, *Bioinformatics*, **36** (2020), 1391–1396. https://doi.org/10.1093/bioinformatics/btz757

22. C. Wu, L. Chen, A model with deep analysis on a large drug network for drug classification, *Math. Biosci. Eng.*, **20** (2023), 383–401. https://doi.org/10.3934/mbe.2023018

23. L. Chen, K. Chen, B. Zhou, Inferring drug-disease associations by a deep analysis on drug and disease networks, *Math. Biosci. Eng.*, **20** (2023), 14136–14157. https://doi.org/10.3934/mbe.2023632

24. L. Chen, J. Xu, Y. Zhou, PDATC-NCPMKL: Predicting drug's Anatomical Therapeutic Chemical (ATC) codes based on network consistency projection and multiple kernel learning, *Comput. Biol. Med.*, **169** (2024), 107862. https://doi.org/10.1016/j.compbiomed.2023.107862

25. M. A. Alsmirat, F. Al-Alem, M. Al-Ayyoub, Y. Jararweh, B. Gupta, Impact of digital fingerprint image quality on the fingerprint recognition accuracy, *Multimedia Tools Appl.*, **78** (2019), 3649–3688. https://doi.org/10.1007/s11042-017-5537-5

26. N. Nedjah, R. S. Wyant, L. M. Mourelle, B. B. Gupta, Efficient fingerprint matching on smart cards for high security and privacy in smart systems, *Inf. Sci.*, **479** (2019), 622–639. https://doi.org/10.1016/j.ins.2017.12.038

27. B. D. Christie, B. A. Leland, J. G. Nourse, Structure searching in chemical databases by direct lookup methods, *J. Chem. Inf. Comput. Sci.*, **33** (1993), 545–547. https://doi.org/10.1021/ci00014a004

28. D. Rogers, M. Hahn, Extended-connectivity fingerprints, *J. Chem. Inf. Model.*, **50** (2010), 742–754. https://doi.org/10.1021/ci100050t

29. T. N. Kipf, M. Welling, Semi-supervised classification with graph convolutional networks, *arXiv preprint*, (2016), arXiv:160902907. https://doi.org/10.48550/arXiv.1609.02907

30. X. Wang, M. Liu, Y. Zhang, S. He, C. Qin, Y. Li, et al., Deep fusion learning facilitates anatomical therapeutic chemical recognition in drug repurposing and discovery, *Briefings Bioinf.*, **22** (2021), bbab289. https://doi.org/10.1093/bib/bbab289

31. H. Zhao, Y. Li, J. Wang, A convolutional neural network and graph convolutional network-based method for predicting the classification of anatomical therapeutic chemicals, *Bioinformatics*, **37** (2021), 2841–2847. https://doi.org/10.1093/bioinformatics/btab204

32. X. Y. Pan, H. B. Shen, Inferring disease-associated microRNAs using semi-supervised multi-label graph convolutional networks, *Iscience*, **20** (2019), 265–277. https://doi.org/10.1016/j.isci.2019.09.013

33. M. Tsubaki, K. Tomii, J. Sese, Compound-protein interaction prediction with end-to-end learning of neural networks for graphs and sequences, *Bioinformatics*, **35** (2019), 309–318. https://doi.org/10.1093/bioinformatics/bty535

34. D. P. Kingma, J. Ba, Adam: A method for stochastic optimization, in *the 3rd International Conference for Learning Representations*, Louisiana, USA, (2019).

35. R. Kohavi, A study of cross-validation and bootstrap for accuracy estimation and model selection, in *IJCAI'95: Proceedings of the 14th International Joint Conference on Artificial Intelligence-Volume 2*, (1995), 1137–1145.

36. D. Powers, Evaluation: From precision, recall and F-measure to ROC, informedness, markedness & correlation, *J. Mach. Learn. Technol.*, **2** (2011), 37–63.

37. F. Huang, Q. Ma, J. Ren, J. Li, F. Wang, T. Huang, et al., Identification of smoking associated transcriptome aberration in blood with machine learning methods, *BioMed Res. Int.*, **2023** (2023), 5333361. https://doi.org/10.1155/2023/5333361

38. H. Wang, L. Chen, PMPTCE-HNEA: Predicting metabolic pathway types of chemicals and enzymes with a heterogeneous network embedding algorithm, *Curr. Bioinf.*, **18** (2023), 748–759. https://doi.org/10.2174/1574893618666230224121633

39. J. Ren, Y. Zhang, W. Guo, K. Feng, Y. Yuan, T. Huang, et al., Identification of genes associated with the impairment of olfactory and gustatory functions in COVID-19 via machine-learning methods, *Life*, **13** (2023), 798. https://doi.org/10.3390/life13030798

40. L. Chen, X. Zhao, PCDA-HNMP: Predicting circRNA-disease association using heterogeneous network and meta-path, *Math. Biosci. Eng.*, **20** (2023), 20553–20575. https://doi.org/10.3934/mbe.2023909

41. L. Chen, Y. Chen, RMTLysPTM: Recognizing multiple types of lysine PTM sites by deep analysis on sequences, *Briefings Bioinf.*, **25** (2024), bbad450. https://doi.org/10.1093/bib/bbad450

42. L. Chen, R. Qu, X. Liu, Improved multi-label classifiers for predicting protein subcellular localization, *Math. Biosci. Eng.*, **21** (2024), 214–236. https://doi.org/10.3934/mbe.2024010

43. B. Matthews, Comparison of the predicted and observed secondary structure of T4 phage lysozyme, *Biochim. Biophys. Acta Protein Struct.*, **405** (1975), 442–451. https://doi.org/10.1016/0005-2795(75)90109-9

44. K. B. Walsh, A. E. McKinney, A. E. Holmes, Minor cannabinoids: Biosynthesis, molecular pharmacology and potential therapeutic uses, *Front. Pharmacol.*, **12** (2021), 777804. https://doi.org/10.3389/fphar.2021.777804

45. B. Rezende, A. K. N. Alencar, G. F. de Bem, F. L. Fontes-Dantas, G. C. Montes, Endocannabinoid system: Chemical characteristics and biological activity, *Pharmaceuticals (Basel)*, **16** (2023), 148. https://doi.org/10.3390/ph16020148

46. P. B. Sampson, Phytocannabinoid pharmacology: Medicinal properties of cannabis sativa constituents aside from the "Big Two", *J. Nat. Prod.*, **84** (2021), 142–160. https://doi.org/10.1021/acs.jnatprod.0c00965

47. InMed pharmaceuticals announces commencement of phase 2 clinical trial investigating cannabinol (CBN), a rare cannabinoid, in the treatment of epidermolysis bullosa, InMed Pharmaceuticals Inc., 2021.

48. P. Clayton, M. Hill, N. Bogoda, S. Subah, R. Venkatesh, Palmitoylethanolamide: A natural compound for health management, *Int. J. Mol. Sci.*, **22** (2021), 5305. https://doi.org/10.3390/ijms22105305

49. P. Clayton, S. Subah, R. Venkatesh, M. Hill, N. Bogoda, Palmitoylethanolamide: A potential alternative to cannabidiol, *J. Diet. Suppl.*, **20** (2023), 505–530. https://doi.org/10.1080/19390211.2021.2005733

50. E. B. Russo, Taming THC: Potential cannabis synergy and phytocannabinoid-terpenoid entourage effects, *Br. J. Pharmacol.*, **163** (2011), 1344–1364. https://doi.org/10.1111/j.1476-5381.2011.01238.x

51. W. S. Ho, D. A. Barrett, M. D. Randall, 'Entourage' effects of N-palmitoylethanolamide and N-oleoylethanolamide on vasorelaxation to anandamide occur through TRPV1 receptors, *Br. J. Pharmacol.*, **155** (2008), 837–846. https://doi.org/10.1038/bjp.2008.324

52. A. Mabou Tagne, Y. Fotio, L. Lin , E. Squire, F. Ahmed, T. I. Rashid, et al., Palmitoylethanolamide and hemp oil extract exert synergistic anti-nociceptive effects in mouse models of acute and chronic pain, *Pharmacol. Res.*, **167** (2021), 105545. https://doi.org/10.1016/j.phrs.2021.105545

53. M. H. Bloch, A. Landeros-Weisenberger, J. A. Johnson, J. F. Leckman, A phase-2 pilot study of a therapeutic combination of Delta (9)-Tetrahydracannabinol and Palmitoylethanolamide for adults with Tourette's syndrome, *J. Neuropsychiatry Clin. Neurosci.*, **33** (2021), 328–336. https://doi.org/10.1176/appi.neuropsych.19080178

54. J. Lott, E. M. Jutkiewicz, M. A. Puthenveedu, The synthetic cannabinoid WIN55,212-2 can disrupt the Golgi apparatus independent of cannabinoid receptor-1, *Mol. Pharmacol.*, **101** (2022), 371–380. https://doi.org/10.1124/molpharm.121.000377

55. J. E. Kuster, J. I. Stevenson, S. J. Ward, T. E. D'Ambra, D. A. Haycock, Aminoalkylindole binding in rat cerebellum: Selective displacement by natural and synthetic cannabinoids, *J. Pharmacol. Exp. Ther.*, **264** (1993), 1352–1363.

56. L. Ferraro, M. C. Tomasini, G. L. Gessa, B. W. Bebe, S. Tanganelli, T. Antonelli, The cannabinoid receptor agonist WIN 55,212-2 regulates glutamate transmission in rat cerebral cortex: An in vivo and in vitro study, *Cereb. Cortex*, **11** (2001), 728–733.

57. S. E. O'Sullivan, An update on PPAR activation by cannabinoids, *Br. J. Pharmacol.*, **173** (2016), 1899–1910. https://doi.org/10.1111/bph.13497

58. J. A. Fields, M. K. Swinton, P. Montilla-Perez, E. Ricciardelli, F. Telese, The cannabinoid receptor agonist, WIN-55212-2, suppresses the activation of proinflammatory genes induced by interleukin 1 beta in human astrocytes, *Cannabis Cannabinoid Res.*, **7** (2022), 78–92. https://doi.org/10.1089/can.2020.0128

59. G. T. Carter, S. P. Javaher, M. H. Nguyen, S. Garret, B. H. Carlini, Re-branding cannabis: The next generation of chronic pain medicine, *Pain Manage.*, **5** (2015), 13–21. https://doi.org/10.2217/pmt.14.49

60. J. P. Szaflarski, E. M. Bebin, Cannabis, cannabidiol, and epilepsy--from receptors to clinical response, *Epilepsy Behav.*, **41** (2014), 277–282. https://doi.org/10.1016/j.yebeh.2014.08.135

61. J. K. Fitzpatrick, E. J. Downer, Toll-like receptor signalling as a cannabinoid target in multiple sclerosis, *Neuropharmacology*, **113** (2017), 618–626. https://doi.org/10.1016/j.neuropharm.2016.04.009

62. S. G. Fagan, V. A. Campbell, The influence of cannabinoids on generic traits of neurodegeneration, *Br. J. Pharmacol.*, **171** (2014), 1347–1360. https://doi.org/10.1016/j.neuropharm.2016.04.009

63. D. An, S. Peigneur, J. Tytgat, WIN55,212-2, a dual modulator of cannabinoid receptors and G protein-coupled inward rectifier potassium channels, *Biomedicines*, **9** (2021), 484. https://doi.org/10.3390/biomedicines9050484

64. C. J. Wenthur, B. Zhou, K. D. Janda, Vaccine-driven pharmacodynamic dissection and mitigation of fenethylline psychoactivity, *Nature*, **548** (2017), 476–479. https://doi.org/10.1038/nature23464

65. I. M. Johnson, H. Prakash, J. Prathiba, R. Raghunathan, R. Malathi, Spectral analysis of naturally occurring methylxanthines (theophylline, theobromine and caffeine) binding with DNA, *PLoS One*, **7** (2012), e50019. https://doi.org/10.1371/journal.pone.0050019

66. M. Wepler, J. M. Preuss, T. Merz, O. McCook, P. Radermacher, J. P. Tuckermann, et al., Impact of downstream effects of glucocorticoid receptor dysfunction on organ function in critical illness-associated systemic inflammation, *Intensive. Care Med. Exp.*, **8** (2020), 37. https://doi.org/10.1186/s40635-020-00325-z

67. A. E. Coutinho, K. E. Chapman, The anti-inflammatory and immunosuppressive effects of glucocorticoids, recent developments and mechanistic insights, *Mol. Cell. Endocrinol.*, **335** (2011), 2–13. https://doi.org/10.1016/j.mce.2010.04.005